NASA Contractor Report 3823

Analytical Investigation of Synchrophasing as a Means of Reducing Aircraft Interior Noise

C. R. Fuller

GRANT NAG1-390
AUGUST 1984

NASA

NASA Contractor Report 3823

Analytical Investigation of Synchrophasing as a Means of Reducing Aircraft Interior Noise

C. R. Fuller

Virginia Polytechnic Institute and State University
Blacksburg, Virginia

Prepared for
Langley Research Center
under Grant NAG1-390

National Aeronautics
and Space Administration

**Scientific and Technical
Information Branch**

1984

1. INTRODUCTION

In the last few years considerable interest has arisen over the use of advanced turbo-propeller (ATP) engines in powering passenger aircraft. This interest is mainly due to the possibility of up to 25% saving in fuel consumption over existing turbo-fan engines. However associated with the use of ATP engines are high acoustic levels at the propeller locations due to supersonic tip speeds. There is concern that due to these high source inputs, the interior noise levels of ATP powered aircraft will be excessive, particularly for commercial applications. A compounding problem is that the fundamental harmonic of the propeller noise is typically between 100 to 250 Hz and the long wavelengths at these frequencies tend to render absorptive techniques ineffective.

One method of noise control, synchrophasing, shows a great deal of promise in that sound levels in a test aircraft were reduced by up to 8 dB,[1] without the penalty of an increase in take-off weight that passive means of noise control incur. Synchrophasing, as a means of noise control, involves setting the relative rotational phase of the propellers until the interior noise levels are minimized. Although it has been shown experimentally[1,2] that synchrophasing can be effective, there exists no analytical model of the process and consequently very little physical understanding of the suppression mechanism. For instance, one of the conclusions of Reference 1 is that synchrophasing provides a significant reduction in energy flux at the fuselage exterior rather than a redistribution of energy in the cabin of a Lockheed P-3C. This result is surprising using the simple interference interpretation of previous workers.

The aim of this paper is to investigate analytically the characteristics of synchrophasing. It is hoped that by using a simplified model of an aircraft, the principal mechanisms inherent in the synchrophasing concept can be uncovered. For the analysis presented here, the aircraft fuselage is approximated by an infinite cylindrical shell with typical materials and properties. This model is appropriate in the light of measurements which show that vibration levels on a typical aircraft fuselage decay with distance away from the propeller plane. The acoustic sources of each propeller (in this case a twin-engined aircraft) are modelled by dipoles located at the source locations of typical propeller driven aircraft. The advantage of using dipole sources is that the directionality and strength of each source can be adjusted to approximate actual pressure distributions at the fuselage. In other words, this arrangement effectively overcomes the need for complicated propeller radiation theory in the analysis.

The acoustic response of the interior of the shell can then be obtained by writing the shell response in spectral form with forcing functions due to the dipole sources. Spectral equations for the vibrational response of fluid-filled and submerged shells have been previously developed by this author[3]. The dipole source is modelled by two monopole sources located at a very small distance apart with the appropriate relative phase and strength to achieve the required directionality. Relationships for sound radiation from a monopole source located near an infinite cylinder have been developed by James[4] and with a transformation to cylindrical co-ordinates using a special

case of the Bessel function addition theorem they are appropriate to the assumed form of the shell spectral equations. Thus solving the system of equations and applying the inverse transformations enables both the response of the shell and the interior acoustic field to be evaluated for various phase differences between the dipole sources corresponding to the synchrophasing concept. In addition, the radial intensity and the line power flow (defined as power flow per unit length) into the shell are evaluated at the shell wall.

2. ANALYSIS

The cylindrical co-ordinate system and the geometry employed in the analysis is shown in Figure 1. Also shown are the first three circumferential mode shapes of the shell response. The method of analysis will be to first derive the response of the system for one monopole source. The response of the complete system will then be obtained, based on linear superposition, by addition of the response of each monopole source with the appropriate phases, amplitudes and locations.

2.1 The Monopole Source

To obtain the vibrational response of the system shown in Figure 1 to a monopole source located at $r = r_p$, $\theta = 0$ and $x = 0$ it is convenient to express the shell displacements as Fourier transforms, viz.

$$\underset{\sim}{u} = (1/\sqrt{2\pi}) \sum_{n=0}^{\infty} \cos(n\theta) \int_{-\infty}^{\infty} \bar{U}_n \exp[ik_{ns}x - i\omega t + i\pi/2]dk_{ns} \qquad (1a)$$

$$\underset{\sim}{v} = (1/\sqrt{2\pi}) \sum_{n=0}^{\infty} \sin(n\theta) \int_{-\infty}^{\infty} \bar{V}_n \exp[ik_{ns}x - i\omega t]dk_{ns} \qquad (1b)$$

$$\underset{\sim}{w} = (1/\sqrt{2\pi}) \sum_{n=0}^{\infty} \cos(n\theta) \int_{-\infty}^{\infty} \bar{W}_n \exp[ik_{ns}x - i\omega t]dk_{ns} \qquad (1c)$$

and similarly the associated interior acoustic field is,

$$p_i = (\omega^2 \rho_f / \sqrt{2\pi}) \sum_{n=0}^{\infty} \cos(n\theta) \int_{-\infty}^{\infty} \bar{W}_n \left[J_n(k_s^r a) / J_n'(k_s^r a) k_s^r a \right]$$

$$X \exp\left[ik_{ns} - i\omega t \right] dk_{ns} \qquad (2)$$

where n is the circumferential mode number, $\underset{\sim}{u}$, $\underset{\sim}{v}$ and $\underset{\sim}{w}$ are the shell displacements in the axial, tangential and radial directions and k_{ns} is the axial wavenumber (A list of symbols is given in the Appendix).

The pressure field at the shell wall, r = a, associated with an exterior monopole source has been previously derived by James[4] and written in spectral form is,

$$\bar{p}_p = - (2/\sqrt{2\pi}) \, p_o \varepsilon_n \, H_n(k_s^r r_p) / H_n'(k_s^r a) k_s^r a$$

$$+ \rho_f \, \omega^2 \, \bar{W}_n \, H_n(k_s^r a) / H_n'(k_s^r a) k_s^r a \qquad (3)$$

where the monopole amplitude p_o has the units of force per unit length and the factor $\varepsilon_n = 1$ for $n = 0$ and $\varepsilon_n = 2$ for $n > 0$. The radial wavenumber k_s^r will be defined shortly.

Equation (3) was derived by using a special case of the Bessel additional theorem to write the free-field pressure of the monopole source in a form appropriate to cylindrical co-ordinates. The presence of the shell wall was then accounted for by introducing a

pressure scattering term corresponding to the normal mode radiation of the shell wall and the unknown amplitudes solved for by applying the boundary condition of continuity of momentum at the shell wall.

Substitution of Equations (1), (2) and (3) into the equations of motion of the fluid loaded shell previously derived in Reference 3 gives the spectral equations of motion of the forced displacement response of the system to the monopole source,

$$\begin{bmatrix} L_{11} & L_{12} & L_{13} \\ L_{21} & L_{22} & L_{23} \\ L_{31} & L_{32} & L_{33} \end{bmatrix} \begin{bmatrix} \bar{U}_n \\ \bar{V}_n \\ \bar{W}_n \end{bmatrix} = \begin{bmatrix} 0 \\ 0 \\ S_{31} \end{bmatrix} \tag{4}$$

where the elements of the matrix system are,

$$L_{11} = -\Omega^2 + (k_{ns}a)^2 + \tfrac{1}{2}(1 - \nu)n^2 \tag{5a}$$

$$L_{12} = \tfrac{1}{2}(1 + \nu)n\ (k_{ns}a) \tag{5b}$$

$$L_{13} = \nu(k_{ns}a) \tag{5c}$$

$$L_{21} = L_{12} \tag{5d}$$

$$L_{22} = -\Omega^2 + \tfrac{1}{2}(1 - \nu)\ (k_{ns}a)^2 + n^2 \tag{5e}$$

$$L_{23} = n,\ L_{31} = L_{13},\ L_{32} = L_{23} \tag{5f, 5g, 5h}$$

$$L_{33} = -\Omega^2 + 1 + \beta^2\left[(k_{ns}a)^2 + n^2\right]^2 - FL \tag{5i}$$

and the source term is given by,

$$S_{31} = (2/\sqrt{2\pi})\ \varepsilon_n\ p_o\left[H_n(k_s^r r_p)/H_n'(k_s^r a)k_s^r a\right]\ \left[\Omega^2/\rho_s\omega^2 h\right] \tag{6}$$

In Equations (5) and (6), Ω is non-dimensional frequency $\Omega = \omega a/C_L$, C_L is the extensional phase speed of the shell material, a is the mean radius of the shell, ν is the Poisson's ratio of the shell material and β is the thickness parameter given by $\beta^2 = h^2/12a^2$ where h is the shell wall thickness.

The fluid loading term due to the normal mode response of the contained fluid and the corresponding normal mode radiation pressure load is,

$$FL = \Omega^2(\rho_f/\rho_s)\ (h/a)^{-1}\ (k_s^r a)^{-1}$$

$$X\ \left[J_n(k_s^r a)/J_n'(k_s^r a) - H_n(k_s^r a)/H_n'(k_s^r a)\right] \tag{7}$$

where ρ_f and ρ_s are the densities of the fluid and shell media respectively. The non-dimensional radial wavenumber can be obtained from the wavenumber vector relationship,

$$k_s^r a = \pm\left[\Omega^2(C_L/C_f)^2 - (k_{ns}a)^2\right]^{1/2} \tag{8}$$

where C_f is the free wave speed of the fluid.

Applying matrix theory to solve the system of Equations (4) enables the spectral radial displacement amplitude to be written as,

$$\bar{W}_n = (2/\sqrt{2\pi})\ \varepsilon_n\ p_o\left[H_n(k_s^r r_p)/H_n'(k_s^r a)k_s^r a\right]\ \left[\Omega^2/\rho_s\omega^2 h\right] I_{33} \tag{9}$$

where I_{33} is the (3,3) element of the inverse of matrix L given by,

$$I_{33} = (L_{11}\ L_{22} - L_{12}\ L_{21})/\det\ |L| \tag{10}$$

Application of the inverse transform of Equation (1c) gives the radial displacement as,

$$\underset{\sim}{w}(x/a,\theta) = p_o\left[\Omega^2/\pi\rho_s ha\omega^2\right] \sum_{n=0}^{\infty} \varepsilon_n \cos(n\theta) \int_{-\infty}^{\infty} \left[H_n(k_s^r r_p)/H_n'(k_s^r a)k_s^r a\right]$$

$$X\ I_{33}\ \exp\left[i(k_{ns}a)(x/a)\right]\ d(k_{ns}a) \tag{11}$$

Similarly the inverse transform of Equation (2) provides the interior acoustic pressure,

$$p_i(r/a,x/a,\theta) = p_o(\Omega^2/\pi\rho_s ha\omega^2)\rho_f\omega^2 a \sum_{n=0}^{\infty} \varepsilon_n \cos(n\theta) \int_{-\infty}^{\infty} \left[H_n(k_s^r r_p)/H_n'(k_s^r a)k_s^r a\right]$$

$$X\ \left[J_n(k_s^r r)/J_n'(k_s^r a)k_s^r a\right]\ I_{33}\ \exp\left[i(k_{ns}a)(x/a)\right]d(k_{ns}a) \tag{12}$$

2.2 The Synchrophase Model

To investigate the characteristics of synchrophasing, the acoustic source at each propeller is modelled by a dipole. The synchrophase angle then corresponds to the phase difference between the dipole sources. The dipoles are constructed from two monopole sources located a small distance apart. The complete arrangement is shown in Figure 1.

The response of the system, based on linearity, can then be considered as a superposition of the response of the system to each monopole source. Thus the total shell response for the system shown in Figure 1 is,

$$
\begin{aligned}
&\underset{\sim}{w}_{total} \Big/ (p_{o_1}/a)\,[\Omega^2/\pi\rho_s h\omega^2] \\
&= \exp[i\phi_1] \sum_{n=0}^{\infty} \varepsilon_n \cos(n\theta) \int_{-\infty}^{\infty} K_w(x/a,\, R_1)\, d(k_{ns}a) \\
&+ (p_{02}/p_{01}) \exp[i\phi_2] \sum_{n=0}^{\infty} \varepsilon_n \cos(n\theta - n\theta_2) \int_{-\infty}^{\infty} K_w(x/a,\, R_2)\, d(k_{ns}a) \\
&+ (p_{03}/p_{01}) \exp[i\phi_3] \sum_{n=0}^{\infty} \varepsilon_n \cos(n\theta - n\theta_3) \int_{-\infty}^{\infty} K_w(x/a,\, R_3)\, d(k_{ns}a) \\
&+ (p_{04}/p_{01}) \exp[i\phi_4] \sum_{n=0}^{\infty} \varepsilon_n \cos(n\theta - n\theta_4) \int_{-\infty}^{\infty} K_w(x/a,\, R_4)\, d(k_{ns}a) \qquad (13)
\end{aligned}
$$

where the displacement integrand is ,

$$
K_w(x/a,\, r_p) = \left[H_n(k_s^r r_p)/H_n'(k_s^r a)k_s^r a\right] I_{33} \exp[i(k_{ns}a)(x/a)] \qquad (14)
$$

In Equation (13) the monopole sources numbered 1, 2, 3 and 4 are located at (R_1, θ_1), (R_2, θ_2), (R_3, θ_3) and (R_4, θ_4) respectively as shown in Figure 1. The sources also vibrate with an amplitude ratio (respective to source 1) of p_{02}/p_{01}, p_{03}/p_{01} and p_{04}/p_{01} and phase angle leads of ϕ_1, ϕ_2, ϕ_3 and ϕ_4 respectively where the subscripts refer to source number. As the theory developed previously is for a monopole source located at $\theta = 0$, in order to obtain Equation (13), it is necessary to apply an angular co-ordinate transformation to each individual source response function.

Thus the synchrophase angle ϕ_s is the phase difference between the dipoles and is specified by,

$$\phi_s = \phi_3 - \phi_1 \tag{15}$$

A similar relationship can be derived for the interior acoustic field and is,

$$p_{total}/(p_{01}/a)(\rho_f/\rho_s)\Omega^2(h/a)^{-1}\ (1/\pi)$$

$$= \exp[i\phi_1] \sum_{n=0}^{\infty} \varepsilon_n \cos(n\theta) \int_{-\infty}^{\infty} K_p(x/a, R_1)\, d(k_{ns}a)$$

$$+ (p_{02}/p_{01}) \exp[i\phi_2] \sum_{n=0}^{\infty} \varepsilon_n \cos(n\theta - n\theta_2) \int_{-\infty}^{\infty} K_p(x/a, R_2)\, d(k_{ns}a)$$

$$+ (p_{03}/p_{01}) \exp[i\phi_3] \sum_{n=0}^{\infty} \varepsilon_n \cos(n\theta - n\theta_3) \int_{-\infty}^{\infty} K_p(x/a, R_3)\, d(k_{ns}a)$$

$$+ (p_{04}/p_{01}) \exp[i\phi_4] \sum_{n=0}^{\infty} \varepsilon_n \cos(n\theta - n\theta_4) \int_{-\infty}^{\infty} K_p(x/a, R_4)\, d(k_{ns}a) \tag{16}$$

where the pressure integrand is,

$$K_p(x/a,\ r_p,\ r) =$$

$$\left[H_n(k_s^r r_p)/H_n'(k_s^r a)k_s^r a\right]\ \left[J_n(k_s^r r)/J_n'(k_s^r a)k_s^r a\right]\ I_{33}$$

$$X\ \exp\left[i(k_{ns}a)(x/a)\right] \qquad (17)$$

3. RESULTS

In order to evaluate the shell response, the interior acoustic field and related variables it is necessary to evaluate the integrals in Equations (13) and (16). The integrands in these equations are transcendental functions with poles and branch points either on or very close to the real axis of the complex $k_{ns}a$ plane. The most convenient method of solution is to numerically evaluate the inverse transform integrals along the real axis. To avoid the singularities located on the integral path, damping is introduced both into the shell material and the fluid field. This has the effect of shifting the poles and branch points of the real axis. Structural damping is introduced by replacing the Young's Modulus E by $E(1 - i\eta_s)$ where η_s is the loss factor of the shell material. Fluid damping is introduced by changing the free speed of propagation C_f of the fluid to $C_f(1 - i\eta_f)$ where η_f is the fluid loss factor. Small values of loss factor were chosen (typically $\eta_s = 0.02$ and $\eta_f = 0.001$) and found to have an insignificant effect on the final result, their presence essentially conditions the integrands for numerical evaluation. The integral was evaluated by using Simpson's rule on a

CYBER computer located at NASA Langley Research Center. The mesh size was chosen to be fine (typically $\Delta k_{ns}a = 0.001$) in order to accurately evaluate the integrand function near the singularities. The integral was also truncated at a finite value of $\pm k_{ns}a$ determined so as to include all the poles and branch points and such that the integrand contribution after the truncation point is small. This method of evaluation of the shell response integral is similar to that used by Y. N. Liu of D.T.N.S.R.D.C. (personal communication).

The following results were calculated for a representative aircraft situation similar to that investigated by Mixson et al.[5] The shell material was taken to be aluminium with a non-dimensional wall thickness of $h/a = 0.001$. The propagating medium was assumed to be air. Material properties are given in Table I. The sources at each propeller location were set as pure dipoles, thus $\phi_2 - \phi_1 = \phi_3 - \phi_4 = \pi$ and were located such that $\theta_1 = \theta_2 = 0$ and $\theta_3 = \theta_4 = \pi$ at a non-dimensional radial distance of $R_1/a = R_2/a = 3.0$ and $R_2/a = R_4/a = 3.1$. The non-dimensional frequencies investigated were chosen to be $\Omega = 0.2$ and 0.14 which, for example, corresponds to frequencies of 219 Hz and 153 Hz in a fuselage of diameter 150 cm. It is in this range of frequencies that the first propeller harmonic usually occurs.

3.1 Sound Pressure Level Reduction

Figures 2 to 5 show the predicted amount of reduction in sound pressure level at various interior locations for differing synchrophase angles between the dipole sources. The results were derived using Equation (17) and are presented so as to be normalized to the maximum sound pressure level obtained at each position.

The results of Figure 2 are for $x/a = 0$, $\theta = 0$, $\Omega = 0.2$ and three different radial points and thus represent sound pressure levels in the "propeller plane" of the interior. It can be seen that the sound levels at each point can be significantly reduced if the correct synchrophase angle is chosen consistent with previous results obtained in practice.[1] It is also apparent that as the observation point moves toward the shell wall, that the optimum synchrophase angle and the degree of attenuation changes. This behaviour can be understood by considering the radial response of the shell wall. Each dipole source excites a series of circumferential modes in the shell which in turn, couple, via the momentum boundary condition, to the interior acoustic field. The acoustic pressure at points inside the shell thus consists of a varying (with cylindrical co-ordinate) superposition of circumferential modes due to the spatial variation in amplitude of each mode. If one considers the dipole sources in phase (i.e. zero synchrophase angle) then all odd circumferential modes will be suppressed while if the dipole sources are 180° out of phase then all even modes are suppressed. For the results of Figure 2, the dominant <u>acoustic</u> mode excited by one dipole source is the $n = 2$ mode with a significant contributions from either the $n = 1$ or $n = 3$ mode depending upon radial location. Hence the optimum synchrophase angle will be close to 180° but will vary with location depending upon the modal composition of the acoustic field at that point. At $r/a = 0$ only the $m = 0$ mode is present thus the optimum synchrophase angle is exactly 180° and the degree of obtainable attenuation in decibels is theoretically infinite at this location. At other radial locations the degree of attenuation obtained is finite for similar reasons as just discussed.

The results of Figure 3 are for $\theta = 30°$. Increasing the observation angle has the effect of causing the curves for differing radial locations to collapse towards the result obtained at $r/a = 0$. Figure 4 presents similar results except at $\theta = 90°$. At this location all odd circumferential modes have a node and thus the optimum synchrophase angle is 180° independent of radial location. Similarly the amount of available attenuation is theoretically infinite. An alternative way of interpreting this situation is that the diagonal $\theta = \pi/2, 3\pi/2$ is a line of symmetry between the sources and thus the optimum synchrophase angle for zero sound pressure level is 180°.

Figure 5 presents synchrophase attenuation curves for $x/a = 10$, $\theta = 0$, $\Omega = 0.2$ and are thus at locations well out of the "propeller plane" and the associated near-field of the sources. Again at $r/a = 0$ the optimum synchrophase angle is 180°. For differing radial locations the optimum synchrophase angle varies markedly, more so than at $x/a = 0$. Similarly the degree of attenuation available in the far-field at differing radial locations can be seen to be far less than that obtained in the "propeller plane," presented in Figure 2. Similar behaviour was observed in synchrophasing experiments performed in a Lockheed P3-C discussed in Reference 1. The behaviour was thought to be due to the acoustic modes having an axial variation in phase (due to differing phase velocities) as well as a spatial variation in amplitude. This increases the number of parameters to be optimized for sound reduction and consequently reduces the degree to which the sound levels can be minimized.

When the source frequency is changed to $\Omega = 0.14$ the synchrophase attenuation curves presented in Figure 6 are markedly different, except for $r/a = 0$. The optimum synchrophase angle in this case is close to zero degrees, however its actual value again varies with radial location. At a frequency of $\Omega = 0.14$, the $n = 1$ circumferential mode dominates the interior acoustic field and thus the optimum synchrophase angle is close to zero degrees. Hence optimum synchrophase angle also varies with frequency due to the changing modal response (or input mode impedance) of the system with frequency.

3.2 Shell Radial Amplitude

Also of interest is the vibrational motion of the shell wall at different synchrophase angles. Although for noise annoyance considerations one would minimize sound pressure levels in the interior, structural vibrations at seating points, etc., will also contribute towards passenger discomfort and thus should also be minimized if possible. Figure 7 shows the predicted radial displacement amplitudes of the shell, obtained from Equation (13) for differing angles of θ and at $x/a = 0$, $\Omega = 0.2$. The synchrophase angle ϕ_s is zero. The amplitudes are plotted so as to be normalized to the maximum calculated value. The response of the shell can be seen from Figure 7 to be a complex superposition of circumferential modes and appears to be dominated by the $n = 4$ mode. When the synchrophase angle is changed to $\phi_s = 180°$, the shell response changes dramatically, as seen in Figure 8. The amplitude distribution curves predict that there will be a node at $\theta = \pi/2$ and $\theta = 3\pi/2$. This effect arises because at a synchrophase angle of 180° all even modes

are suppressed and the remaining odd circumferential modes have nodes at these angles. The response of the shell at this synchrophase angle can be seen to be dominated by the n = 3 mode.

If the total angular response of the shell is known (i.e. as derived from Equation (13)) then the individual amplitude of each circumferential mode can be obtained by utilizing the orthogonality of the cos(nθ) and sin(nθ) distribution functions.

Writing the shell response as,

$$\underset{\sim}{w} = \sum_{n=0}^{\infty} W_n \cos(n\theta) \exp\left[ik_{ns}x - i\omega t\right]$$

$$+ \sum_{n=1}^{\infty} \bar{W}_n \sin(n\theta) \exp\left[ik_{ns}x - i\omega t\right] \qquad (18)$$

the mode amplitudes at x/a = 0 are given by,

$$W_n = (1/\varepsilon\pi) \int_0^{2\pi} \underset{\sim}{w}_{\text{total}} \cos(n\theta)\, d\theta, \quad n = 0, 1, 2... \qquad (19)$$

and

$$\bar{W}_n = (1/\pi) \int_0^{2\pi} \underset{\sim}{w}_{\text{total}} \sin(n\theta)\, d\theta, \quad n = 1, 2, 3... \qquad (20)$$

where $\underset{\sim}{w}_{\text{total}}$ is specified by Equation (13) and $\varepsilon = 2$ if $n = 0$, $\varepsilon = 1$ if $n \neq 0$. When the source locations are chosen as in this paper then $\bar{W}_n = 0$ for all n. Decomposed circumferential mode amplitudes using Equations (19) and (20) are presented in Table II in

non-dimensional form such that $W_n = W_n^{nd}(p_{01}/a)[\Omega^2/\pi\rho_s h\omega^2]$. The results are calculated at $x/a = 0$ for $\Omega = 0.2$ and two synchrophase angles. When the synchrophase angle is zero, the amplitude of all odd modes are zero as previously discussed, and the shell response is dominated by the $n = 4$ mode. The $n = 2$ mode also has a strong response and this causes the complex vibration pattern presented in Figure 7. Changing the synchrophase angle to 180° leads to all even modes being suppressed and now the shell response is dominated by the $n = 3$ mode. It is also interesting that, as the results presented in Table II are absolute values, it can be seen that the amplitude of the $n = 3$ mode when $\phi_s = 180°$ is greater than the amplitude of the $n = 4$ mode when $\phi_s = 0°$. Figures 2 to 5 predict however that the optimum synchrophase angle for sound level reduction in the same situation is close to 180°, and this is a further illustration of the complexity of the shell-fluid coupling factor inherent in the synchrophase optimization technique. A synchrophase angle chosen to minimize shell vibrations may thus tend to enhance the sound pressure level of the interior acoustic field.

3.3 Radial Intensity and Power Flow at the Shell Wall

The radial intensity was calculated using the time averaged intensity equation,

$$I(x/a,\theta) = \frac{1}{2}\ \mathrm{Re}[p\ X\ (\dot{\underset{\sim}{w}})^*] \qquad (21)$$

where the acoustic pressure at the shell wall was calculated from

Equation (16). The shell radial velocity was obtained from Equation (13) utilizing $\underset{\sim}{w} = -i\omega\underset{\sim}{w}$.

The radial intensity vectors calculated at the shell wall are presented in Figure 9 where $x/a = 0$, $\Omega = 0.2$ and the synchrophase angle is zero, i.e. the dipole sources are in phase. The magnitude of the intensity vector is normalized to the maximum value calculated. The intensity vectors demonstrate that, in the "propeller plane" when $\phi_s = 0$, most of the acoustic energy enters through the shell in localized "hot spots" close to each source. This behaviour is surprising considering the long wavelength (relative to shell diameter) of the source sound field. What is also surprising is that there are regions where acoustic energy <u>leaves</u> the shell near $\theta = \pi/2$ and $3\pi/2$.

When the synchrophase angle is changed to $\phi_s = 180°$ the associated intensity vectors change dramatically as shown in Figure 10. Now it can be seen that the acoustic energy enters the shell in regions close $\theta = \pi/4$, $3\pi/4$, $5\pi/4$ and $7\pi/4$, and subsequently flows out of the shell in regions close to each source. The net power flow into the shell is still positive. To understand the physics of Figure 10 it is necessary to remember that the intensity is time averaged and thus in real time the vectors oscillate in magnitude. Thus at the beginning of the harmonic cycle the energy flows from one dipole source, say at $\theta = 0$, through regions of the shell close to $\theta = \pi/4$ and $7\pi/4$ into the interior. Now as the other source is 180° out of phase it acts as an acoustic sink and the acoustic energy then flows <u>out</u> of the shell close to $\theta = \pi$. As the harmonic cycle progresses

the situation reverses and the energy flows in the opposite direction. In other words the presence of the dipole with a synchrophase angle of 180° causes the shell wall impedance in the source near field to fall markedly and thus sound can easily transmit through the wall in this region.

The line acoustic power flow (i.e. power flow per unit length of shell) into the interior of the shell can be obtained by integrating the radial intensity at the shell wall with respect to $ad\theta$. Figure 11 presents the non-dimensional line acoustic power such that

$$P = -P^{nd}(1/2\pi)\ (p_{01}/a)^2\ \Omega^4\ (\rho_f/\rho_s)\ (h/a)^{-2}\ \omega^{-1}\ \rho_s^{-1}$$

at different locations along the shell axis for a synchrophase angle of $\phi_s = 0$, $\Omega = 0.2$. The most interesting result of Figure 11 is that it demonstrates that most of the acoustic energy (for one direction of propagation) enters the shell in a length equal to one shell diameter from the "propeller plane". This localized flow of energy is due to the region of the shell surface being in the source near-field where the forcing pressures are very high. It is also surprising to see that there is a length of shell immediately after the in-flow region where a significant amount of energy flows out of the shell. No reason for this behaviour has been put forward so far but it was thought to be most likely due to radiation from that part of the shell vibrational near-field that has long wavelengths.

At large distances from the "propeller plane" the line power flow is much less but still out of the shell. Thus the acoustic energy enters the shell in a localized area centered on the "propeller plane" and then propagates as duct modes to locations away from the "propeller plane". As the shell has a high impedance relative to air

these duct modes propagate with only slight attenuation. However at large values of x/a the exterior acoustic field due to direct radiation from the dipole sources is small and thus the interior acoustic field energy radiates out to the external field via shell coupled motion.

Figure 12 shows the calculated reduction in line power at the propeller plane for various synchrophasing angles for two frequencies $\Omega = 0.2$ and 0.14. The optimum synchrophase angle for minimum input power flow for $\Omega = 0.2$ is close to $180°$ indicating most of the power is carried by shell vibration in even circumferential modes. When the source frequency is changed to $\Omega = 0.14$ the optimum synchrophase angle is close to 0 degrees because of the high response of the $n = 3$ mode. However in this case the available reduction in line power is far less than for $\Omega = 0.2$.

4. CONCLUSIONS

An analysis has been presented by which the acoustic and structural response of a shell-fluid system excited by two dipole sources can be obtained in a closed form solution. The arrangement is representative of a propeller driven aircraft. The parameters of sound pressure level distribution, shell radial displacement amplitude and energy flow into the interior has been evaluated for differing phase angles (i.e. the synchrophase effect) between the dipole sources. The results obtained have been used to investigate and explain the mechanisms behind the synchrophase effect. A number of important conclusions have been obtained as follows:

1. Synchrophasing has been shown to theoretically provide significant sound level and shell vibration reduction.

2. The optimum synchrophase angle changes with interior location and frequency and may be different for suppression of the interior acoustic field than suppression of the shell response or acoustic power flow into the shell. Thus choice of the optimum synchrophase angle will ultimately depend upon a choice of one of the above criteria or a compromise between all of them.

3. The maximum achievable amount of attenuation of the interior acoustic field changes with location and frequency, however it is greatest in the "propeller plane".

4. Conclusions 1 to 3 are very similar to results actually measured in a Lockheed P3-C[1] and thus serve to validate the model and its associated approximations presented in this paper.

5. Acoustic energy enters and leaves the shell in localized areas or "hot spots." The location of the "hot spots" changes dramatically with the synchrophase angle. This result tends to suggest the localized use of either acoustic or vibrational active control applied at the shell wall to obtain even greater sound or structural vibration attenuation. An alternative to active control may be the localized use of passive control methods. However care must be taken to apply this only where energy enters the shell. Application in other areas may reduce sound attenuation.

6. The great majority of the acoustic energy enters the interior of the shell in a length of one shell diameter (for one direction of propagation) and propagates to other locations as interior duct

modes. This implies that any form of additional noise control should only be applied in a fuselage diameter either side of the "propeller plane." A substantial amount of energy was found to flow out of the shell in a region located greater than one diameter from the "propeller plane." It may be possible to enhance this effect for interior sound control away from the "propeller plane."

7. The shell response is fundamental to the transmission mechanism due to its circumferential standing wave response and associated coupling behaviour with the contained acoustic field. Thus models for noise transmission into aircraft fuselages based on flat or finite curved plates are inadequate for low frequencies. Similarly models based on random or plane wave incidence of sound in which there are no source directivity characteristics (i.e. similar to architectural acoustics) are very likely to lead to spurious results.

5. REFERENCES

1. Johnston, J. L., Donham, R. E. and Guinn, W. A.: "Propeller Signatures and Their Use." AIAA Paper 80-1035, 1980.

2. Magliozzi, B.: "Synchrophasing for Cabin Noise Reduction of Propeller - Driven Aircraft." AIAA Paper 83-0717, 1983.

3. Fuller, C. R.: "The Input Mobility of an Infinite Circular Cylindrical Elastic Shell Filled with Fluid." Journal of Sound and Vibration, Vol. 87, No. 3, 1983, pp. 409-427.

4. James, J. H.: "Computations of Acoustic Power, Vibration Response and Acoustic Pressures of Fluid-filled Pipes." Admiralty Marine Technology Establishment (U.K.) Technical Memorandum TM 82036, 1982.

5. Mixson, J. S., Barton, C. K., Piersol, A. G. and Wilby, J. F.: "Characteristics of Propeller Noise on an Aircraft Fuselage Related to Interior Noise Transmission." AIAA Paper 79-0646, 1979.

APPENDIX

List of Symbols

a	shell mean radius
c_f	fluid free speed of propagation
c_L	shell free speed of propagation
E	Young's Modulus
FL	fluid loading term
h	shell wall thickness
I	intensity
I_{33}	(3,3) element of inverse matrix
k_s^r	radial wavenumber
k_{ns}	axial wavenumber
K_p	pressure integrand
K_w	displacement integrand
ℓ	source index number
L	matrix term
n	circumferential mode number
p_i	acoustic pressure of interior field
$\bar{p}_p$	spectral pressure due to monopole source

P_o — pressure amplitude of monopole source

P — acoustic power

P^{nd} — non-dimensional acoustic power, $P/(1/2\pi)\ (P_{o_1}/a)^2\ \Omega^4\ (\rho_f/\rho_s)\ (h/a)^{-2}\omega^{-1}\rho_s^{-1}$

r
Θ
x — cylindrical co-ordinate

r_p — radial location of monopole source

R_ℓ — radial location of dipole source component

S — matrix source term

t — time

$\left.\begin{matrix}\underset{\sim}{u}\\ \underset{\sim}{v}\\ \underset{\sim}{w}\end{matrix}\right\}$ — shell displacement vectors

$\left.\begin{matrix}\overline{U}\\ \overline{V}\\ \overline{W}\end{matrix}\right\}$ — shell spectral displacement amplitudes

W_n^{nd} — non-dimensional shell radial displacement amplitude, $\overline{W}/(P_{o_1}/a)\left[\Omega^2/\pi p_s h\omega^2\right]$

β — shell thickness parameter

ε — $\begin{cases} = 2 & \text{if } n = 0 \\ = 1 & \text{if } n > 0 \end{cases}$

ε_n — $\begin{cases} = 1 & \text{if } n = 0 \\ = 2 & \text{if } n > 0 \end{cases}$

ϕ_ℓ	phase lead of dipole source component
ϕ_s	synchrophase angle
θ_ℓ	angular location of dipole source component
ρ_f	density of fluid field
ρ_s	density of shell material
η_f	fluid loss factor
η_s	shell loss factor
Ω	non-dimensional source frequency, $\omega a/C_L$
ω	source frequency (rad/sec)
ν	Poisson's ratio
(*)	complex conjugate

TABLE I

Material Properties

Material	Young's Mod. N/m^2	Poisson's Ratio	Density kg/m^3	Free Wave Speed m/s	η_t, η_f
Aluminum	7.1×10^{10}	0.33	2700	5150	0.02
Air	-----	----	1.2	343	0.001

TABLE II

Non-dimensional Circumferential Mode Amplitudes W_n, $x/a = 0$, $\Omega = 0.2$

Circumferential Mode Number, n

	0	1	2	3	4	5	6	7	8	9
$\phi_s = 0$	0.39×10^{0}	0	0.43×10^{1}	0	0.67×10^{1}	0	0.60×10^{0}	0	0.25×10^{-1}	0
$\phi_s = 180$	0	0.29×10^{1}	0	1.0×10^{2}	0	2.31×10^{1}	0	0.13×10^{0}	0	0.45×10^{-2}

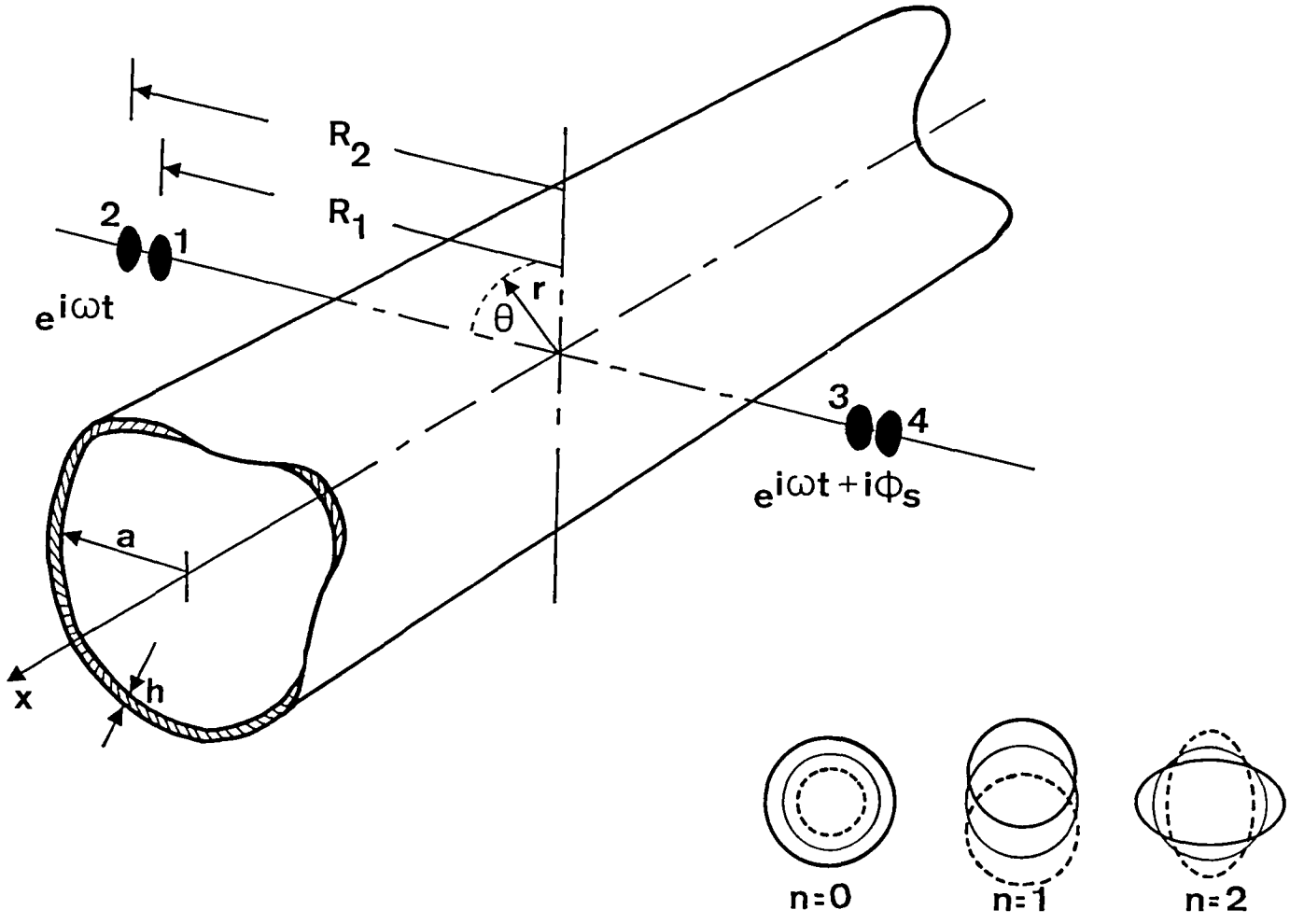

Figure 1. Geometry, co-ordinate system and modal shapes.

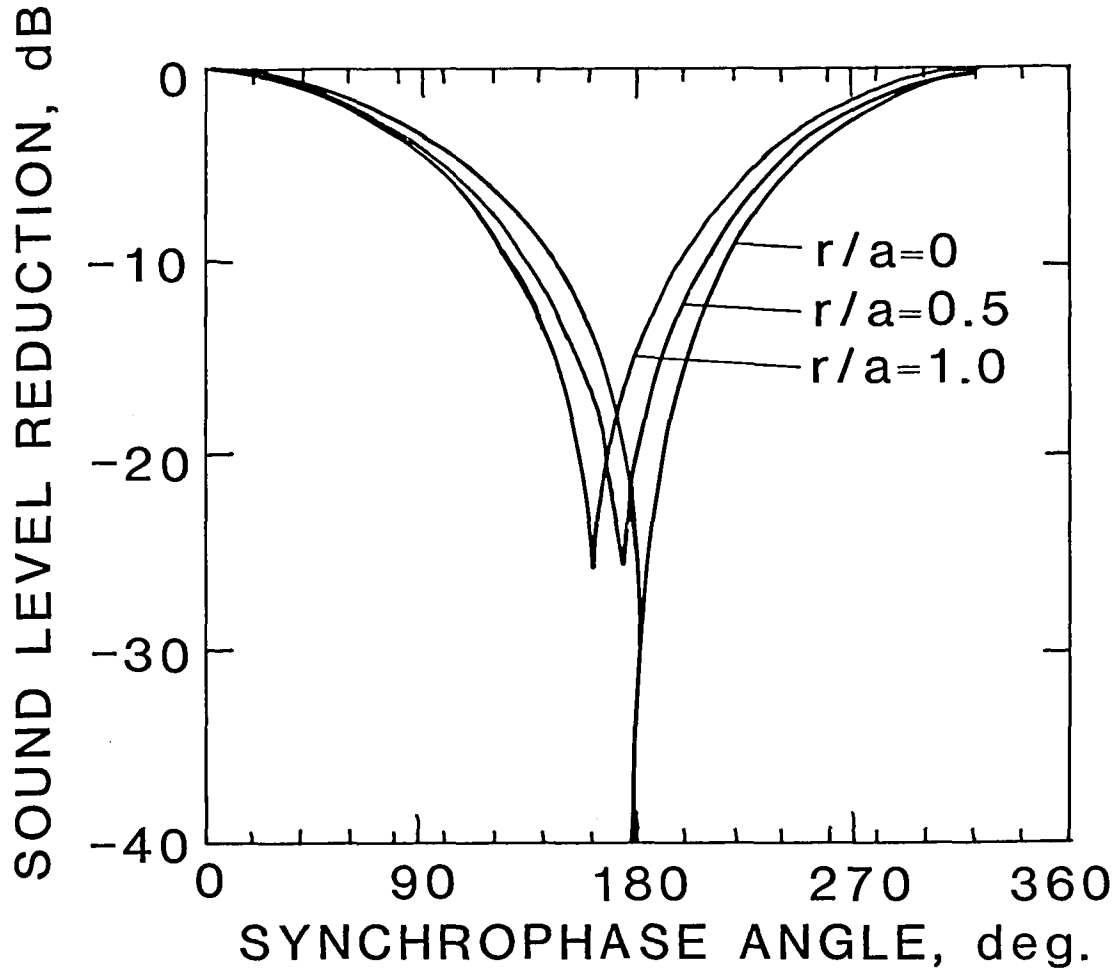

Figure 2. Sound level reduction at x/a = 0, θ = 0, Ω = 0.2

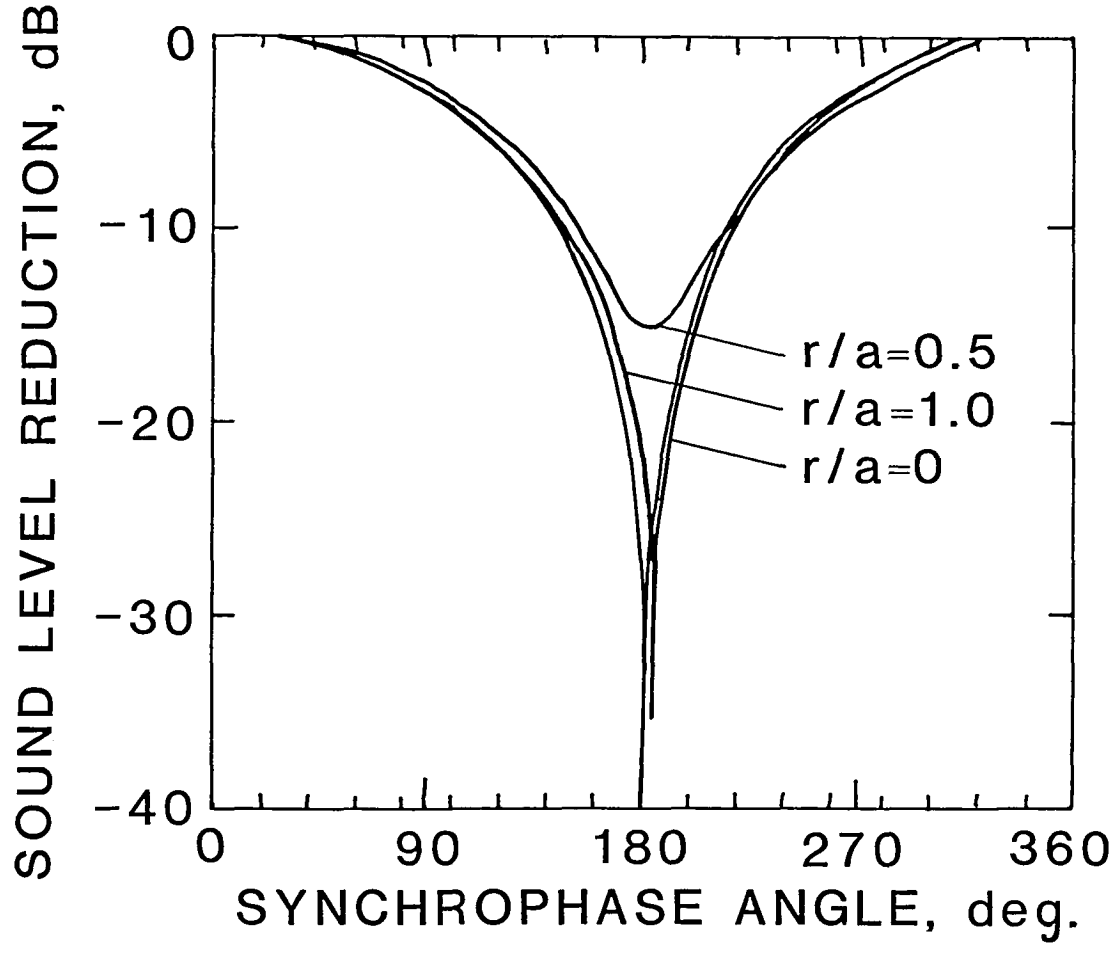

Figure 3. Sound level reduction at x/a = 0, θ = 30, Ω = 0.2

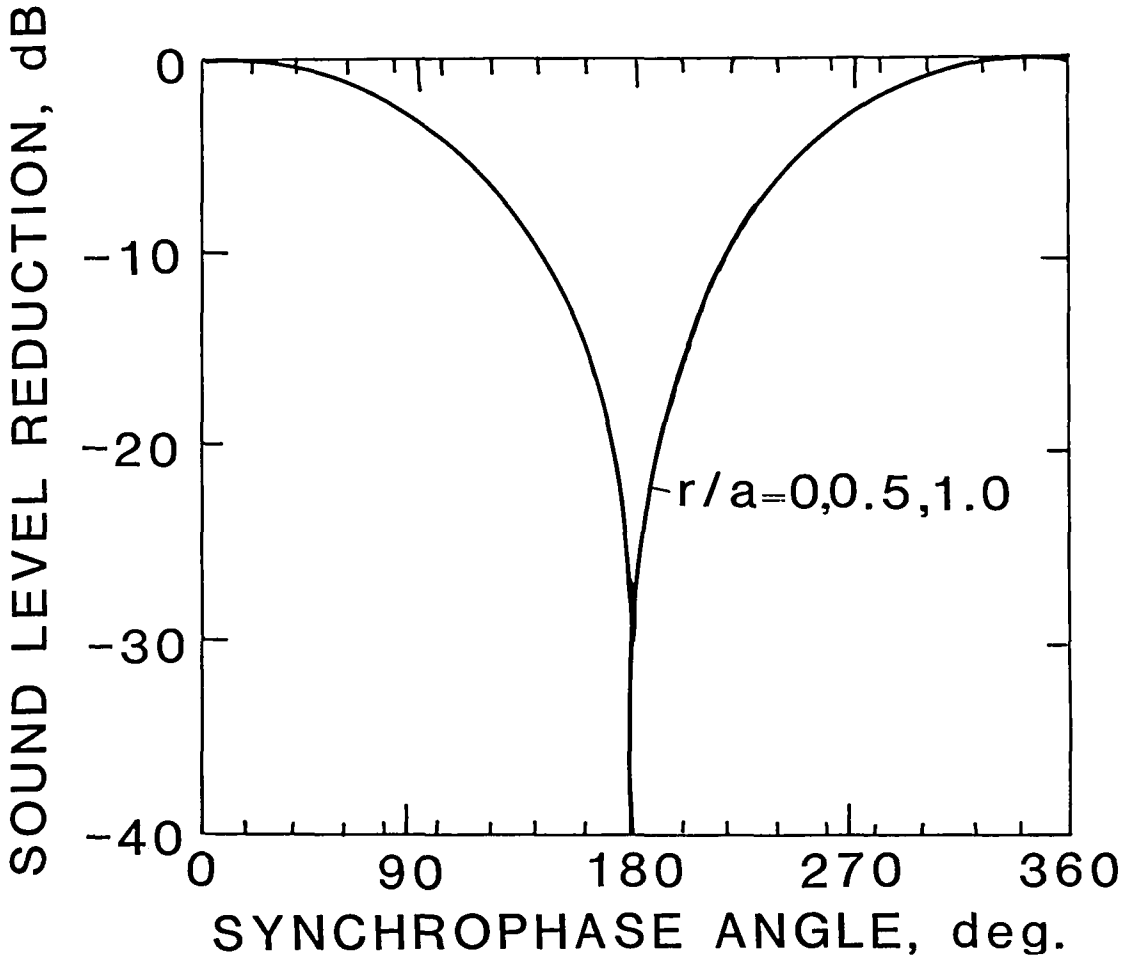

Figure 4. Sound level reduction at x/a = 0, θ = 90, Ω = 0.2

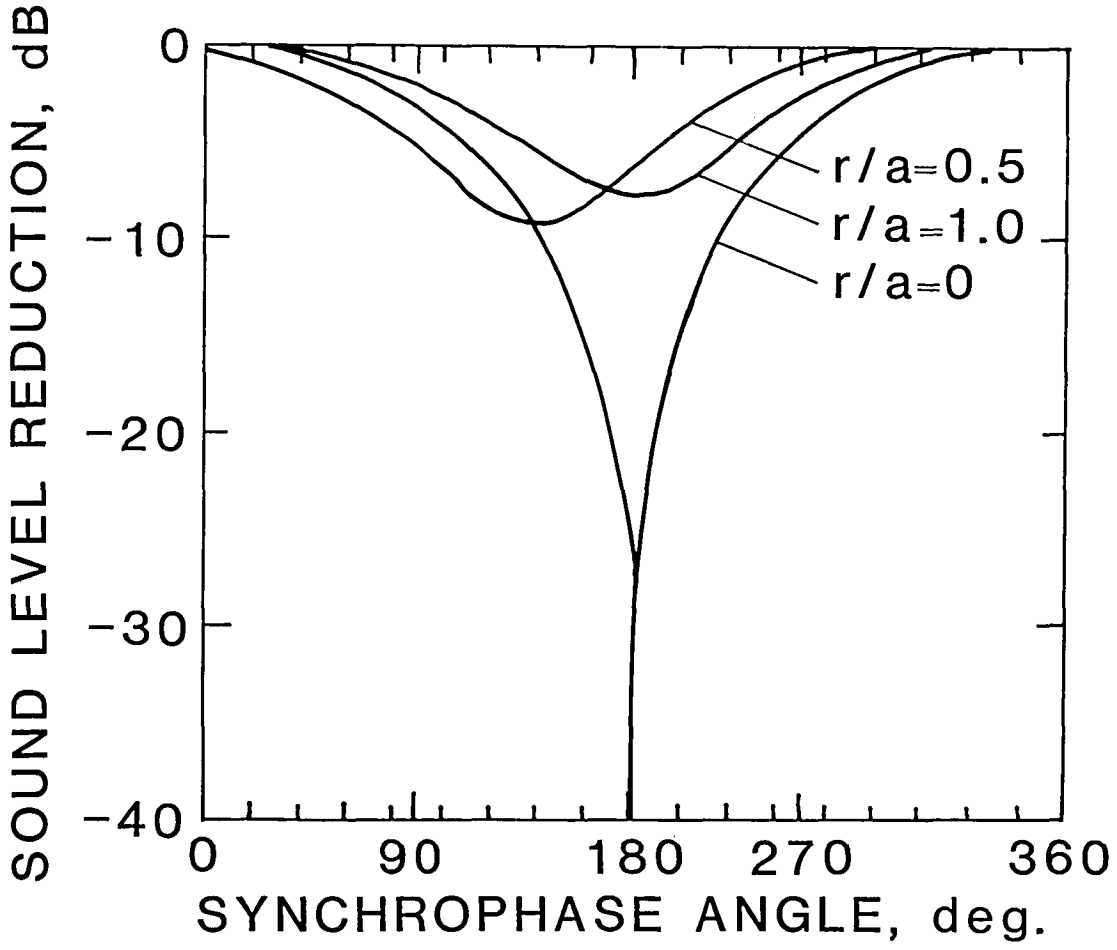

Figure 5. Sound level reduction at x/a = 10, θ = 0, Ω = 0.2

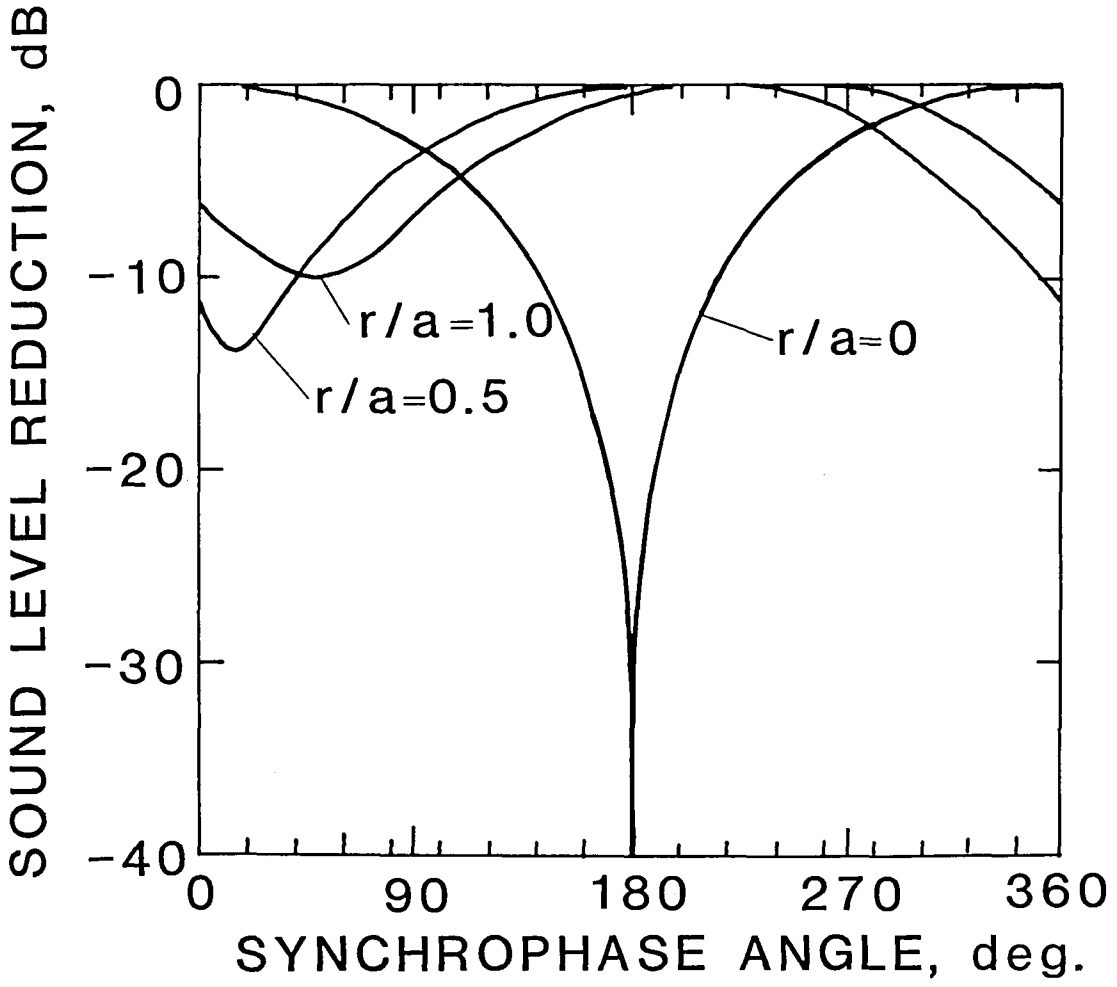

Figure 6. Sound level reduction at x/a = 0, θ = 0, Ω = 0.14

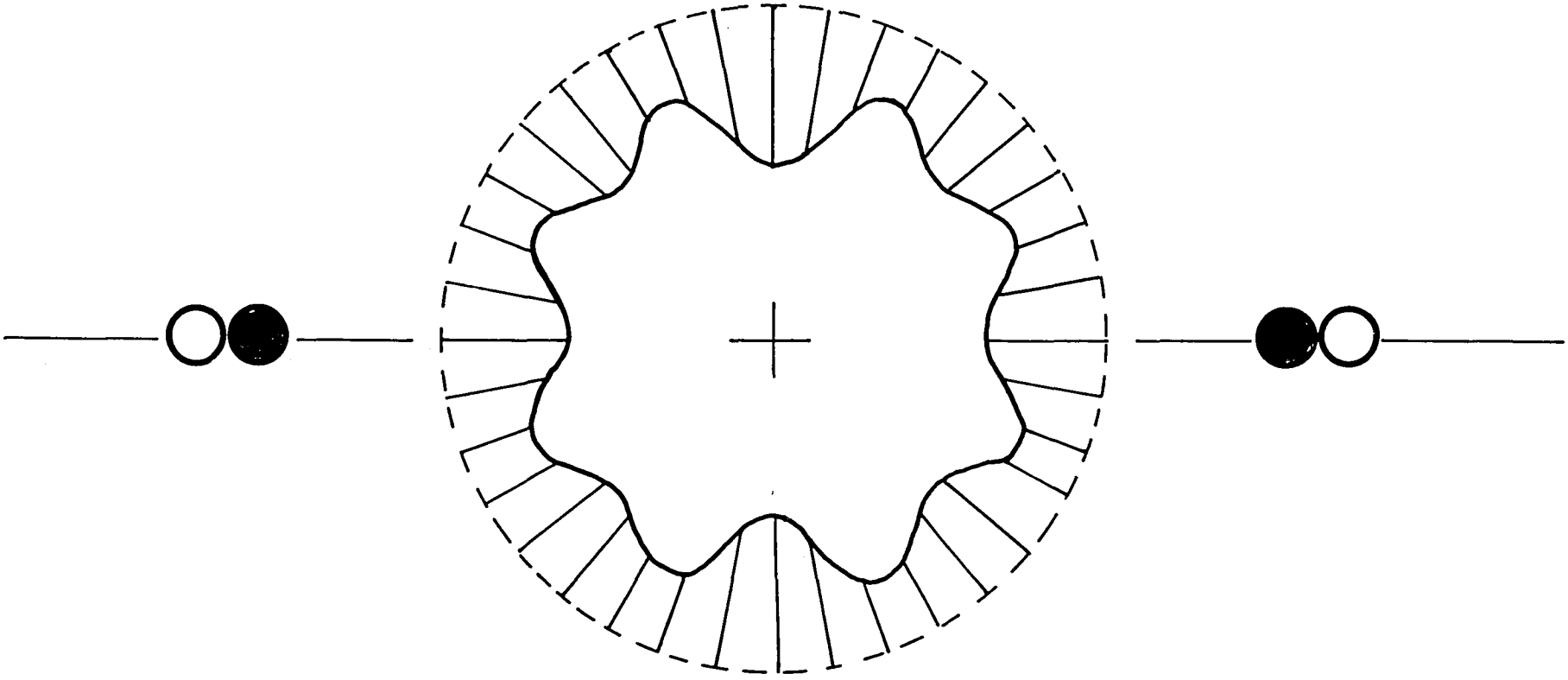

Figure 7. Normalized radial displacement amplitude, x/a = 0, $\phi_s = 0$, $\Omega = 0.2$.;-----, shell undisturbed; ———, shell displacement.

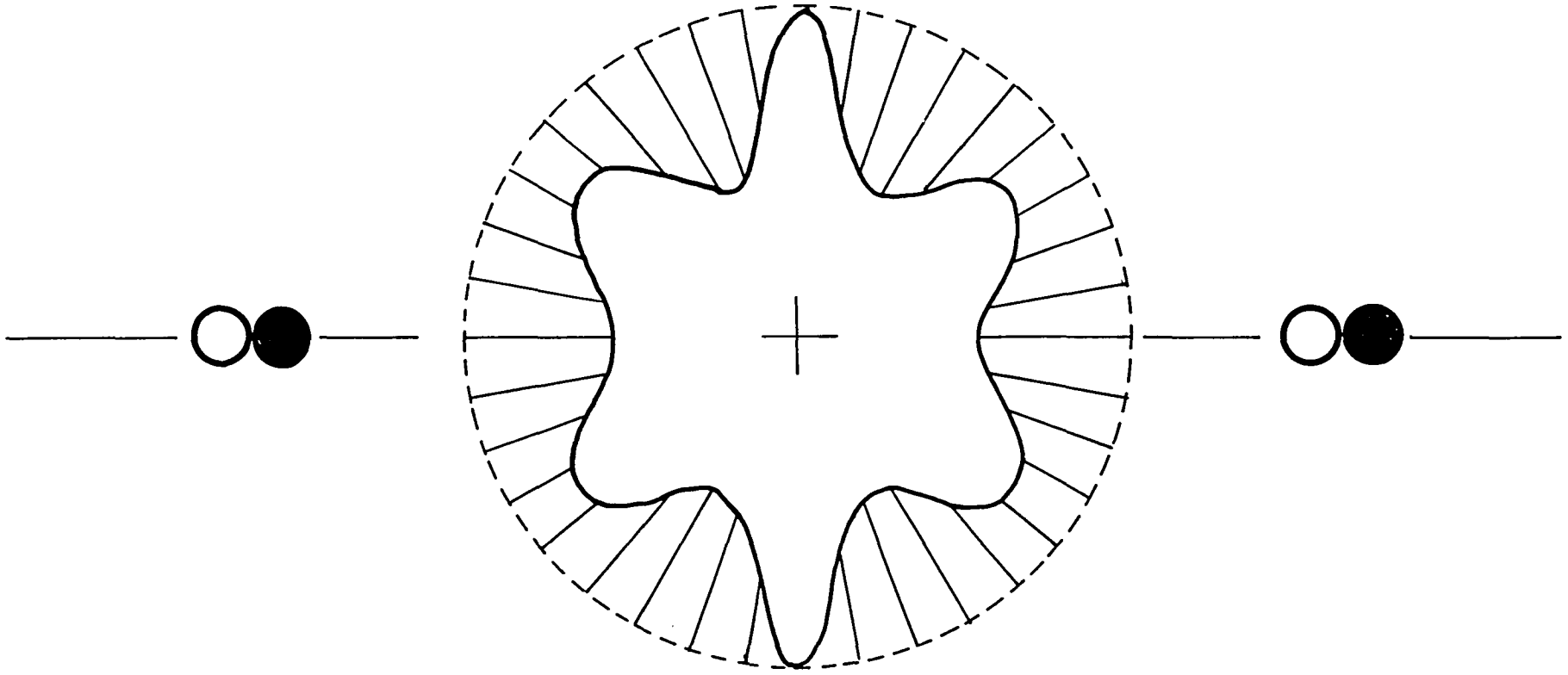

Figure 8. Normalized radial displacement amplitude, x/a = 0, ϕ_s = 180, Ω = 0.2. ;-----, shell undisturbed;———, shell displacement

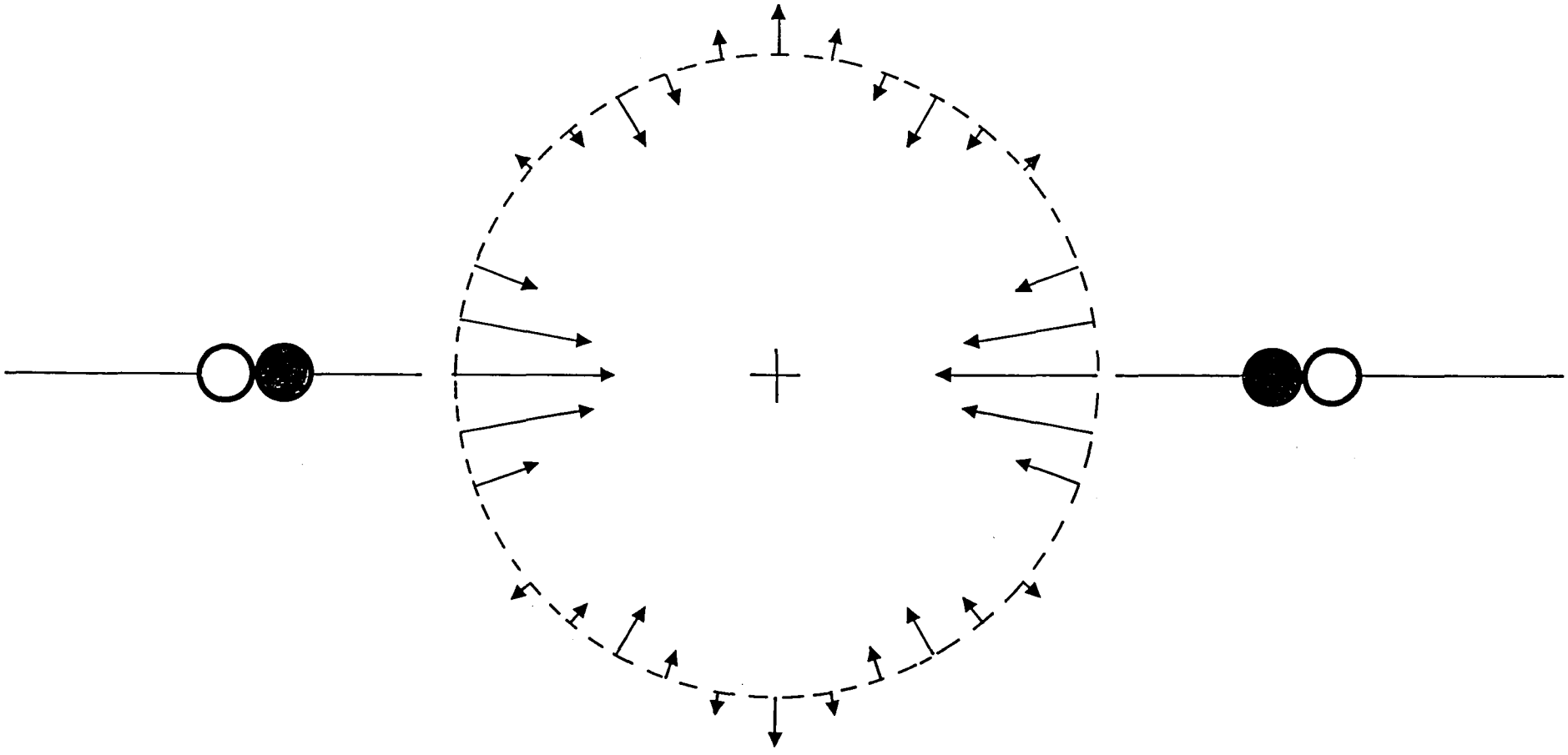

Figure 9. Normalized radial intensity at shell wall, $x/a = 0$, $\phi_s = 0$, $\Omega = 0.2$.

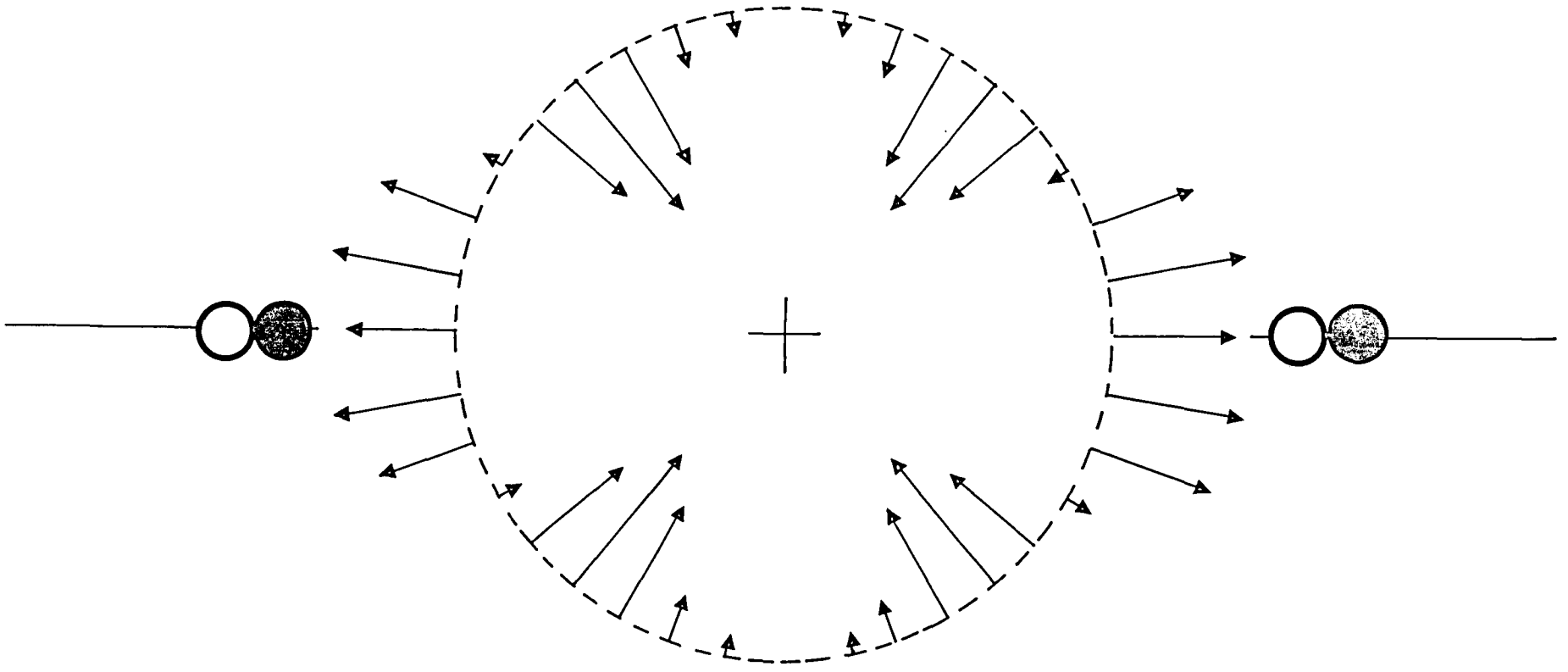

Figure 10. Normalized radial intensity at shell wall, $x/a = 0$, $\phi_s = 180$, $\Omega = 0.2$.

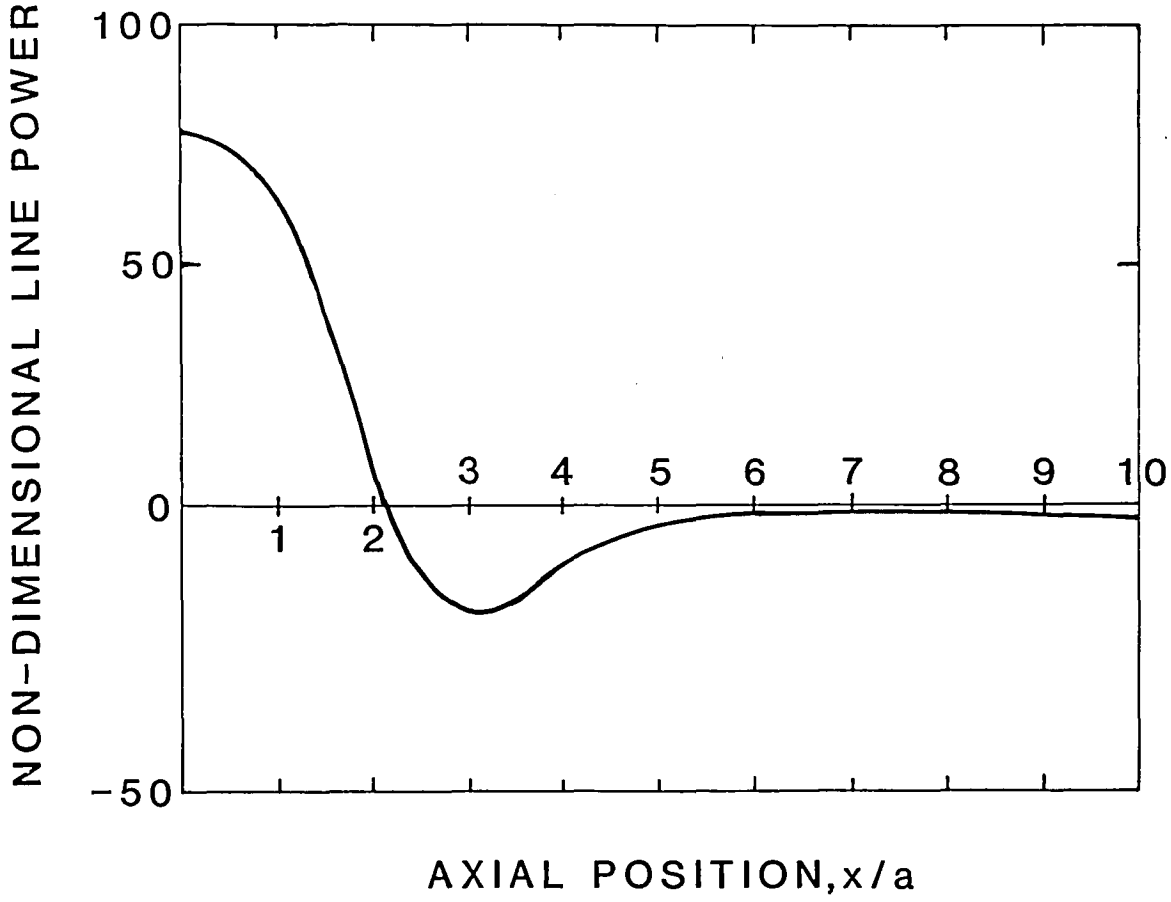

Figure 11. Non-dimensional line power flow at shell wall, $\phi_s = 0$, $\Omega = 0.2$

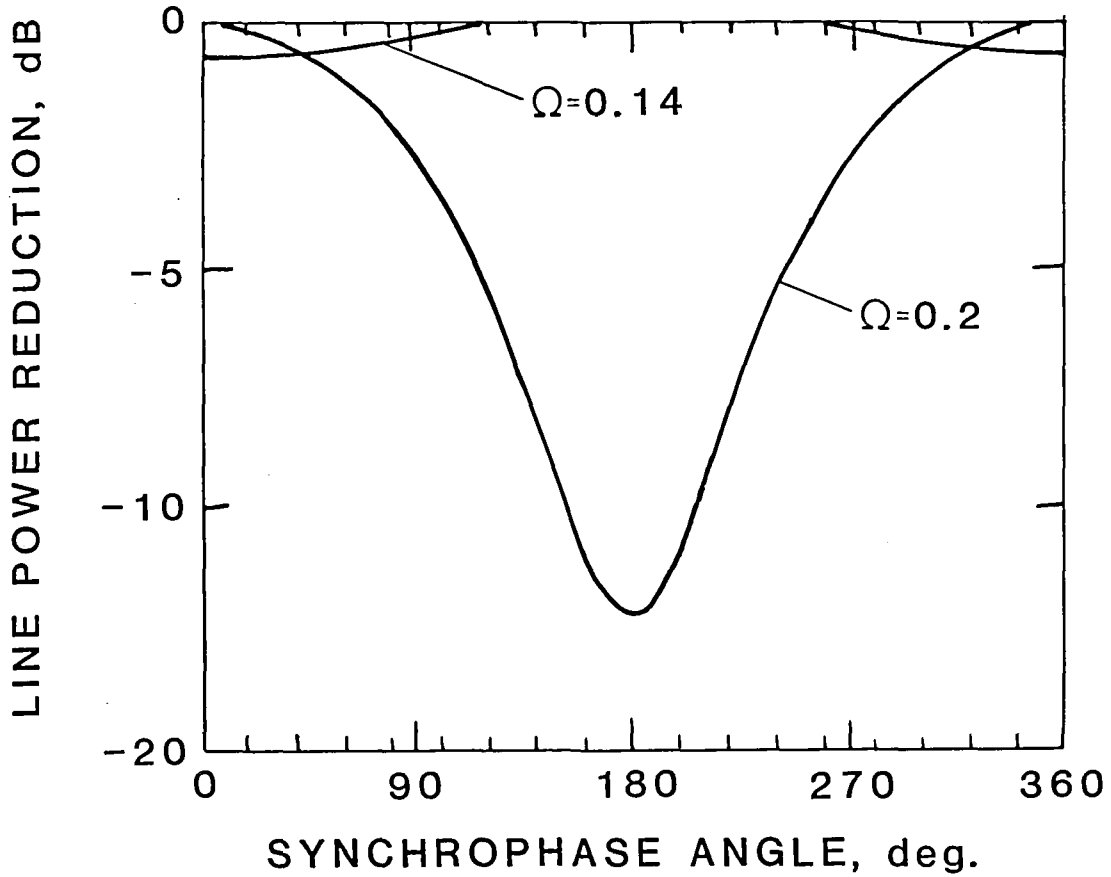

Figure 12. Line power reduction at shell wall, x/a = 0.

1. Report No.	2. Government Accession No.	3. Recipient's Catalog No.
NASA CR-3823		

4. Title and Subtitle	5. Report Date
ANALYTICAL INVESTIGATION OF SYNCHROPHASING AS A MEANS OF REDUCING AIRCRAFT INTERIOR NOISE	August 1984
	6. Performing Organization Code
7. Author(s)	8. Performing Organization Report No.
C. R. Fuller	
	10. Work Unit No.
9. Performing Organization Name and Address	11. Contract or Grant No.
Virginia Polytechnic Institute and State University Department of Mechanical Engineering Blacksburg, VA 24061	NAG1-390
	13. Type of Report and Period Covered
12. Sponsoring Agency Name and Address	Contractor Report
National Aeronautics and Space Administration Washington, DC 20546	14. Sponsoring Agency Code

15. Supplementary Notes

Langley Technical Monitor: David Chestnutt

16. Abstract

In this report the noise control characteristics of synchrophasing are investigated using a simplified model of an aircraft fuselage. The analysis presented here includes directivity effects of the noise sources and solves in closed form the coupled motion between the interior and exterior acoustic fields and the shell vibrational response. The variation in sound pressure level at various locations inside the shell is studied for various synchrophase angles as well as the shell vibrational response and input power flow in order to uncover the principal mechanisms behind the transmission phenomena.

17. Key Words (Suggested by Author(s))	18. Distribution Statement
Interior Noise Synchrophasing Scattering of Sound from Cylinders	Unclassified - Unlimited Subject Category 71

19. Security Classif. (of this report)	20. Security Classif. (of this page)	21. No. of Pages	22. Price
Unclassified	Unclassified	42	A03

For sale by the National Technical Information Service, Springfield, Virginia 22161

NASA-Langley, 1984